

Ordering dynamics of snow under isothermal conditions

H. Löwe,* J. K. Spiegel, and M. Schneebeli

WSL, Institute for Snow and Avalanche Research SLF, Davos, Switzerland

(Dated: November 28, 2018)

We have investigated the morphological evolution of laboratory new snow under isothermal conditions at different temperatures $T = -3, -9, -19^\circ\text{C}$ by means of X-ray tomography. The collective dynamics of the bicontinuous ice-vapor system is monitored by the evolution of the two-point (density) correlation function $C(\mathbf{r}, t)$ and a particular thickness distribution which is similar to a pore size distribution. We observe the absence of dynamic scaling and reveal fundamentally different classes of length scales: The first class comprises the mean ice thickness and the (inverse) specific surface area (measured per ice volume) which increase monotonically and follow a power law. The dynamic exponent is in accordance with coarsening of a locally conserved order parameter. A second class of length scales is derived from the slopes of $C(\mathbf{r}, t)$ at the origin in different coordinate directions. All these scales show a slower growth with anomalous power law scaling. The existence of two different power laws is quantitatively consistent with coarsening of fractal aggregates and reveal the persistence of power law correlations in the initial condition where the snow contains dendritic structures. At low temperatures these structures persist even over an entire year. A third class of length scales can be defined by the first zero crossings of $C(\mathbf{r}, t)$. The zero crossings display a non-monotonic evolution with a strong anisotropy between the direction of gravity and horizontal directions. We attribute this behavior to larger scale structural relaxations of the ice network which apparently leave the small scale interfacial relaxations unaffected. However, vice versa it remains the question how structural mobility is induced by interfacial coarsening.

PACS numbers: 61.43.Gt, 64.75.-g, 83.80.Nb, 81.10.-h

I. INTRODUCTION

Snow crystals exhibit a variety of morphological changes which are driven by fundamentally different, thermodynamic conditions. During growth the problem can be well described by an *isolated* crystal in a supersaturated environment which is a classical problem of single crystal growth [1]. If specifics of the ice crystal lattice are taken into account, orientation dependent growth velocities can be measured [2] and the snow morphology diagram can be reasonably well explained in terms of temperature, supersaturation and lattice properties, see [3] for a review. If these non-equilibrium growth forms are deposited (e.g. on the ground to form a seasonal snowpack) the crystals no longer evolve in isolation. Structural correlations may be built up already during atmospheric aggregation [4] or deposition on the ground [5] where a tenuous ice network is formed. The subsequent evolution of the deposit is then ultimately dominated by *collective* behavior and mutual interactions between the crystals. The simplest case of thermodynamic conditions applied to a snow crystal deposit are isothermal conditions at fixed temperature below zero. The subsequent relaxation of the ice network to equilibrium is commonly referred to as isothermal metamorphism of snow.

The occurrence of isothermal metamorphism in nature is limited to deep polar snowpacks [6]. From the collective dynamics point of view the problem is however of general interest. Previous work focused on possible transport mechanisms as the origin of interfacial relaxation. It is widely believed that evaporation-condensation of vapor is the dominant process of mass transport [7–9]. Experiments are then interpreted in terms grain growth [8], sintering theory [10] or a mean-field approach [9] which is similar to the LSW theory (Lifshitz and Slyozov [11] and Wagner [12]) with screening [13]. For a review we refer to [14]. The dynamical evolution of the ice morphology is usually characterized in terms of a single characteristic length scale l . Widely used is the inverse specific surface area per ice volume [7, 8, 10, 15]. Sometimes an ice thickness is used [10] which is derived from a pore-size like thickness distribution. Another length scale observed during isothermal metamorphism is the inverse mean curvature as investigated in [15, 16]. However, there is no agreement about the dynamic exponents z which governs the growth law $l \sim t^{1/z}$. Recent Monte Carlo simulations [17] confirm power law behavior between 2 and 4 with a strong variation with temperature. Some work suggest a logarithmic growth $l \sim \ln(t)$ [8] at intermediate times. Most of the work investigates natural snow samples which resist to reveal a concise picture of the dynamics.

*loewe@slf.ch

To address the values of the exponents and a possible origin of the scattering it is instructive to first resort to certain idealized pictures with universal features as a reference. Given the evaporation-condensation mechanism, snow as an ice-vapor mixture in a non-equilibrium state will relax to equilibrium by capillarity driven coarsening [18]. Neglecting gravity for a moment, it is widely accepted [19] that basically two different universality classes are likely to occur in phase ordering systems: For a locally conserved order parameter, all length scales l in the system will evolve with $z = 3$ whereas the locally non-conserved case leads to $z = 2$. Note, that the specification of evaporation-condensation as the dominant transport mechanism alone does not ultimately determine the dynamic exponent: Depending on whether the dynamics is limited by intermediate diffusion or the interface reaction the order parameter is effectively locally or globally conserved, respectively. Both cases are treated in LS [11] whereas W only considers the globally conserved case [12]. The picture is however neither limited to isolated droplet-like structures nor to infinite dilution as in LSW. Both universality classes are also found in simulations of the late stage evolution of (symmetric) bicontinuous structures as exemplified by the Cahn–Hilliard or Allen–Cahn equation [20]. In both cases *dynamic scaling* scaling holds and the system is truly characterized by a single diverging length scale. Within this idealized picture snow should end up with $z = 2$ or $z = 3$. Additionally any of the commonly investigated quantities such as specific surface area, mean or Gaussian curvature can be equally likely used as the characteristic length scale to determine the dynamic exponent z .

Indeed, real systems almost always display deviations from ideality. This is a consequence of emerging, competing length scales. The origin of additional scales can roughly be distinguished into the following classes: i) transient behavior from initial conditions which involve intrinsic non-short ranged correlations, ii) the emergence of intermediate dynamic regimes which are governed by different scaling laws. Both lead to a an apparent breakdown of dynamic scaling under experimental conditions. For snow it is likely that both effects will play a role. The most unambiguous measure to detect the presence (or absence) of dynamic scaling are the rescaling properties of length distribution functions. Amongst others the most prominent candidate is the equal time, two-point (or pair) correlation function $C(\mathbf{r}, t)$ of the microscopic density $\rho(\mathbf{x}, t)$. Its importance stems from the fact that its Fourier transform, the structure factor is directly accessible by scattering experiments of inhomogeneous media [21] without explicit knowledge of the microscopic density $\rho(\mathbf{x}, t)$. In addition two-point correlation functions are a general starting point for systematic approaches to physical properties of heterogeneous materials [22].

The focus of the present paper is a multiple-scale characterization of the isothermal evolution of snow from its collective dynamics point of view, which is probed by fluctuations of the microscopic density field $\rho(\mathbf{x}, t)$. We use X-ray tomography to measure $\rho(\mathbf{x}, t)$ with high resolution throughout an entire year for different temperatures and characterize the dynamics by means of the density correlation function. Surprisingly, this has not been investigated before. To better control the initial conditions we use laboratory snow with crystals grown from vapor which are subsequently deposited into sample holders by sieving. By comparing the evolution of various length scales we are able to identify different mechanisms which contribute to the breakdown of dynamic scaling. These mechanisms are likely to be active simultaneously in natural snow samples.

The paper is organized as follows. The experimental setup is described in Section II. In Section III we define the correlation function and a thickness distribution from which various length scales are derived. The measurement results for the observables are presented in Section IV. The discussion of all results is done Section V and in the final section VI we give the conclusions and suggestions for future work.

II. EXPERIMENTS

Our general experimental setup for the X-ray tomography basically follows [10], with two important differences for the sample handling: i) the isothermal storage was improved to minimize the effect of predominant temperature gradients, ii) laboratory-generated new snow is used to guarantee similar initial conditions for the snow samples at different temperatures. Details are given below.

A. Snow sample preparation

All snow samples were prepared from “nature-identical” laboratory snow which was produced in a simple snowmaker as described below. The design basically follows [23]: A heated water reservoir is kept at warm temperature of $T = 30^\circ\text{C}$ in a cold room environment at ambient room temperature of $T = -25^\circ\text{C}$. The humid air above the water surface is continuously advected (by a fan) into box at ambient temperature where the vapor precipitates at thin nylon wires which serve as growth nuclei. By varying air and water temperature the method is able to qualitatively reproduce growth modes and crystal habits predicted by the snowflake morphology diagram [3]. Under the conditions described above, mainly dendritic structures are generated. Snow crystals are periodically harvested from the wires

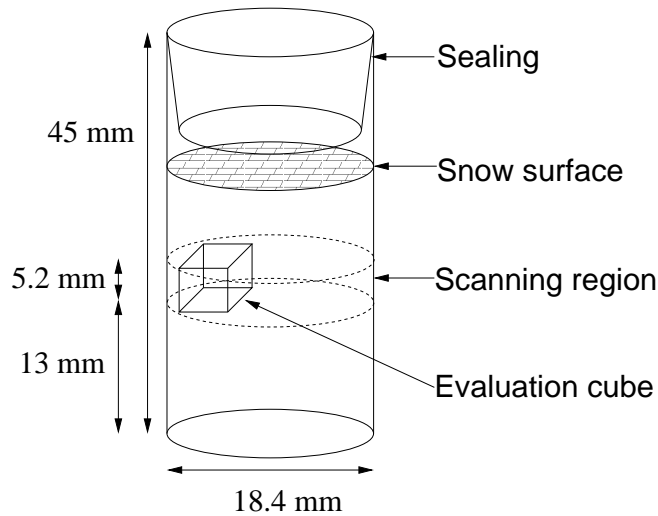


FIG. 1: Schematic of the cylindrical tomography sample holder.

by automatic vibrations of the wires. The so obtained snow powder compact had a density of $\rho \approx 172 \text{ kg m}^{-3}$. With an ice density of $\rho_{\text{ice}} = 917 \text{ kg m}^{-3}$ this amounts to initial volume fractions of $\phi_i = 0.188$. The snow was stored for 24 h at $T = -25^\circ\text{C}$ to allow for moderate, initial sintering of the crystals. Using a sieve with mesh size of 2 mm, the snow was sieved into cylindrical sample holders, cf. Fig 1, until they were completely filled. The snow was then slightly compressed and sealed with a polyethylene cap (PE-LD) to avoid sublimation and obtain a closed environment with respect to mass exchange.

B. Sample storage

To improve the isothermal conditions, the storage boxes used in [10] were improved to reduce thermal gradients. The storage consists of layers of highly insulating and highly conducting materials. The highly conducting material with high heat capacity (steel) prevents the buildup of a temperature inversion in the air, and eliminates temperature fluctuations. From the inside out, the packaging was as follows: The sample cylinders were fixed in a Styrofoam mask inside a steel cylinder with 1 cm thick walls. The steel cylinders were capped from both sides with 1 cm thick steel lids. This steel cover was packed into a small Styrofoam box with 5 cm thick walls. The box was again surrounded by 5 mm thick steel plates and then enclosed in a vacuum box. The temperature was recorded inside each steel cylinder by two temperature sensors (iButtons DS1922L). These sensors have an accuracy of $\pm 0.5^\circ\text{C}$, (from -10°C , to $+65^\circ\text{C}$), and a resolution of 0.0625°C . They were calibrated before the measurements. Recorded temperatures were almost constant with mean values and standard deviations of $T = -3.7 \pm 0.7^\circ\text{C}$, (sample 1), $T = -9.5 \pm 0.1^\circ\text{C}$, (sample 2) and $T = -18.6 \pm 0.8^\circ\text{C}$, (sample 3). This corresponds to a homologous temperature of 0.99, 0.97 and 0.93.

C. Tomography

At the beginning of the experiment each sample is measured roughly in 3 week intervals. Since the evolution slows down during the experiment [10] we decreased the measuring frequency in the late stage of the experiment. For measurements the samples are transported from the storage room to the CT in a small Styrofoam box. We use a commercial μ -CT80 micro-computer-tomograph (CT) from Scanco. The scanning in the CT was done with a nominal resolution (pixel size) of $10 \mu\text{m}$ and a modulation transfer function at 10% contrast level of $12.4 \mu\text{m}$. The scanning region was fixed in space at 13 mm height from the bottom of the sample holder, cf. Fig.1. The height of the scanning region is 5.2 mm (520 voxels). The CT was kept close to the nominal storage temperatures -3 , -9 and -19°C . After the measurement, the sample was placed in the transport box and returned to the storage box.

From the attenuation map of the scanned region a cube of 520^3 voxels = $(5.2 \text{ mm})^3$ was extracted, cf. Fig. 1, which was large enough to be a representative volume for the considered properties [24]. The gray scale images were filtered using a Gaussian filter with kernel-size of 5^3 and standard deviation of 1.2 voxels to improve the signal to noise ratio.

A binary image was then obtained by segmentation of the filtered data. A single segmentation threshold was used for all images. The threshold was determined such that the density of all samples is matched on average.

III. OBSERVABLES

A. Two point correlation function

Appropriate measures to monitor the evolution of the microstructure can be defined from the microscopic density. For continuous mass distributions the microscopic density is defined in terms of the phase indicator function $\phi_i(\mathbf{x})$ of the ice phase which is defined by $\phi_i(\mathbf{x}) = 1$, if \mathbf{x} lies in the ice phase and zero otherwise. The mass density is then related by the intrinsic density of ice $\rho_{\text{ice}} = 917 \text{ kg m}^{-3}$ via

$$\rho_i(\mathbf{x}, t) := \rho_{\text{ice}} \phi_i(\mathbf{x}, t). \quad (1)$$

The simplest first order statistical quantity of a two phase random medium is its volume fraction

$$\phi_i(t) := \overline{\phi_i(\mathbf{x}, t)}. \quad (2)$$

The overbar denotes ensemble averaging. Practically we replace ensemble averages by volume averages and thus implicitly assume a statistically homogeneous system.

The simplest, higher order statistical characterization of a random, two-phase medium is given by the equal-time, two-point correlation function

$$C(\mathbf{r}, t) := \overline{[\phi_i(\mathbf{x} + \mathbf{r}, t) - \phi_i(t)][\phi_i(\mathbf{x}, t) - \phi_i(t)]}. \quad (3)$$

The two-point function $C(\mathbf{r}, t)$ is the continuous counterpart of the pair correlation function of discrete particle assemblies. Note that $C(\mathbf{r}, t)$ does not only depend on the magnitude of \mathbf{r} , thus we explicitly account for anisotropic behavior. Below we will restrict ourselves on the behavior along different coordinate directions and therefore define $C_\alpha(r, t) := C(r \mathbf{e}_\alpha, t)$ for $\alpha = x, y, z$.

From the two-point correlation function various length scales can be defined. For later purposes we follow [25] and define a length scale from the slope of $C(\mathbf{r}, t)/C(0, t)$ at the origin, viz.

$$l_\alpha(t) := - \left(\frac{d}{dr} C_\alpha(r, t) / C_\alpha(0, t) \Big|_{r=0} \right)^{-1}. \quad (4)$$

We note that for isotropic media in spatial dimension $d = 3$ the correlation lengths are related to the specific surface area s per *unit volume* via $\frac{d}{dr} C_\alpha(r, t) \Big|_{r=0} = s/4$ for $\alpha = x, y, z$, cf. [22]. Henceforth the l_α are referred to as interfacial (correlation) lengths.

In bicontinuous materials, such as microemulsions, the covariance is often approximated by oscillatory two-scale forms, e.g. $C(r)/C(0) = \exp(-r/l) \cos(\pi r/(2l_0))$ which involves, besides the interfacial correlation length l another length scale l_0 . The latter determines the first zero crossing of $C(r)$ which is attained at $r = l_0$ and can be given the meaning of a typical domain size. In view of this two-scale approximation we define the first zero crossing

$$l_{0,\alpha}(t) := \min\{r | C_\alpha(r, t) = 0\} \quad (5)$$

as another characteristic length scale, which is referred to the structural (correlation) length henceforth.

Finally, we define the ratio of ice volume and surface area as an additional length scale since it is widely used in snow science,

$$l_{\text{ssa}}(t) := \phi_i(t) / s(t). \quad (6)$$

B. Thickness distribution

Another commonly used distribution of length scales for a porous material has been defined in [26] and is given by the distribution of local thicknesses. Its definition deviates from the common pore-size distribution [22] and can be written as a conditional probability

$$p_{\text{th}}(r, t) := \overline{\delta(r - r_{\text{max}}(\mathbf{x})) \phi_i(\mathbf{x}, t) / \phi_i(t)}, \quad (7)$$

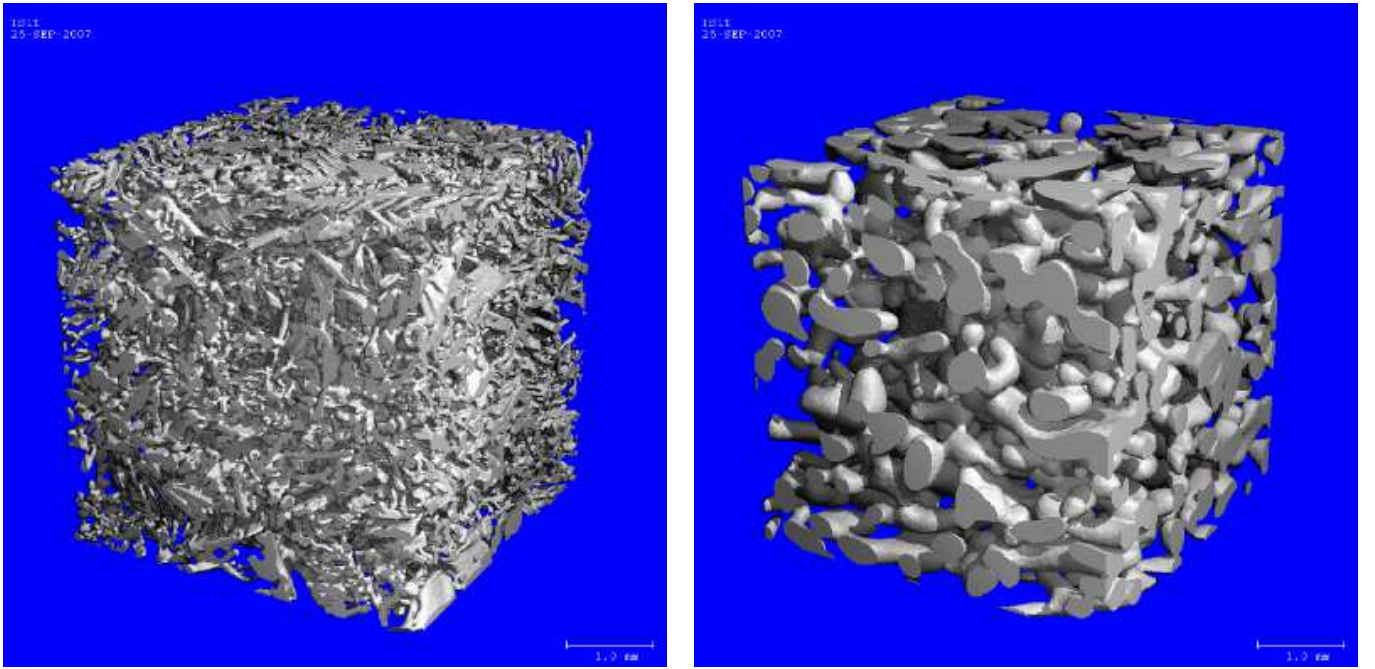


FIG. 2: (Colors online) Evolution of a snow cube at $T = -3^\circ\text{C}$, in the beginning (left), and in the end after almost one year (right). The length of the cube is 5.2 mm.

where $r_{\max}(\mathbf{x})$ is the radius of the largest sphere which i) contains \mathbf{x} (not necessarily as its center) and ii) is itself contained completely in the ice phase. An important implication of this definition of thickness is revealed by the following example. Consider a collection of non-overlapping spheres of radius r_0 . This indeed implies a delta-like thickness distribution $p_{\text{th}}(r) = \delta(r - r_0)$. If the spheres are reshaped (under volume conservation) to a long cylinder of radius r_0 which is terminated by hemi-spherical caps of the same radius at both ends the thickness distribution remains invariant.

As a characteristic length scale of the thickness distribution we use the mean which is given by

$$l_{\text{th}}(t) := \int_0^\infty dr r p_{\text{th}}(r, t). \quad (8)$$

IV. RESULTS

A. Overview

The structural analysis of the snow samples is evaluated within the cubic subsets of the entire sample of size $(5.2\text{mm})^3$, cf. Fig. 1. With a voxel size of $10\mu\text{m}$ this leads to lattice sizes of 520^3 . A visual impression of the three dimensional evolution of the ice-matrix is shown in Fig. 2. The samples evolve from highly branched, fresh snow in the initial conditions to a rounded bicontinuous structure. Warmer samples evolve faster than colder ones.

B. Density

The evolution of the volume fraction given in Eq. (2) of the samples is shown in Fig. 3. Note that the scale is double logarithmic and a guide to the eye is given as a reference for a possible power-law evolution at the late stage. However, the evolution clearly displays deviations from a straight line caused by modulations.

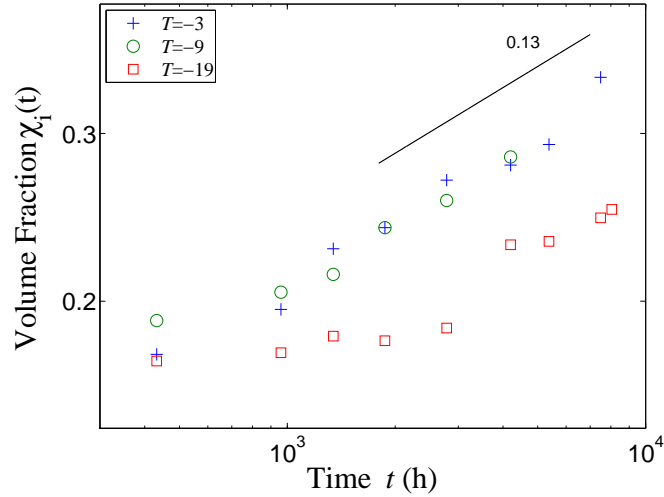


FIG. 3: (Colors online) Temporal evolution of the volume fraction $\phi_i(t)$ at all temperatures.

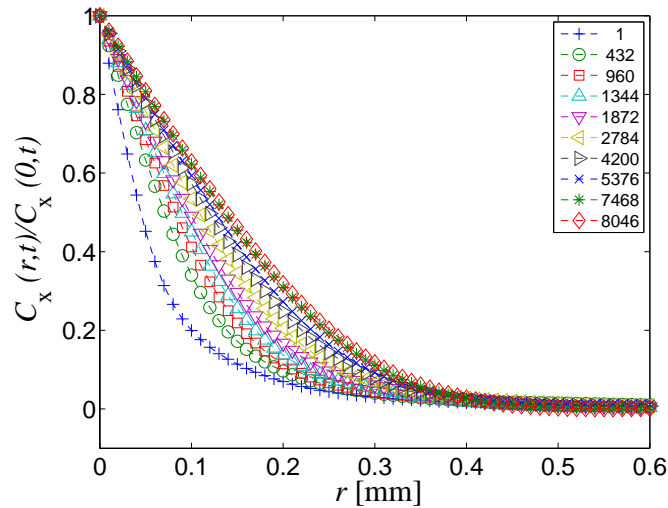


FIG. 4: (Colors online) Evolution of $C_x(r,t)$ at $T = -3^\circ\text{C}$ for different times (in h). On a linear scale the evolution at all temperatures appears to be similar.

C. Two point correlation function

1. Scaling

In the following we follow [25] and normalize the correlation function defined in Eq. (3) by their values at the origin $C_\alpha(r,t)/C_\alpha(0,t)$. An overview of the evolution of the two-point correlation function $C_x(r,t)$ at $T = -3^\circ\text{C}$ is given in Fig. 4. All samples clearly display a cusp singularity at the origin revealing a non-fractal ice-vapor interface on scales $10\mu\text{m}$ throughout the entire experiment. The smooth appearance of the interface on these scales has also been confirmed by a comparison between X-ray tomography and gas absorption (BET) derived surface area [27].

Next we consider the, possibly anisotropic, dynamic scaling and rescale $C_\alpha(r,t)$ by the correlation lengths $l_\alpha(t)$ which are obtained by fitting the cusp at the origin against $C_\alpha(r,t)/C_\alpha(0,t) = 1 - r/l_\alpha(t)$. These slopes increase in the course of time revealing a coarsening of the structure. From the perspective of dynamic scaling the results at $T = -9^\circ\text{C}$ cannot be distinguished from $T = -3^\circ\text{C}$ and thus we concentrate on the comparison between $T = -3^\circ\text{C}$ and $T = -19^\circ\text{C}$. In addition, at both temperatures the x and y directions can be regarded as equivalent and thus we concentrate on the comparison between x and z direction. We explicitly note that z is the direction of gravity.

The results for the rescaled correlation functions at high temperature $T = -3^\circ\text{C}$ are given in Fig. 5, and for the

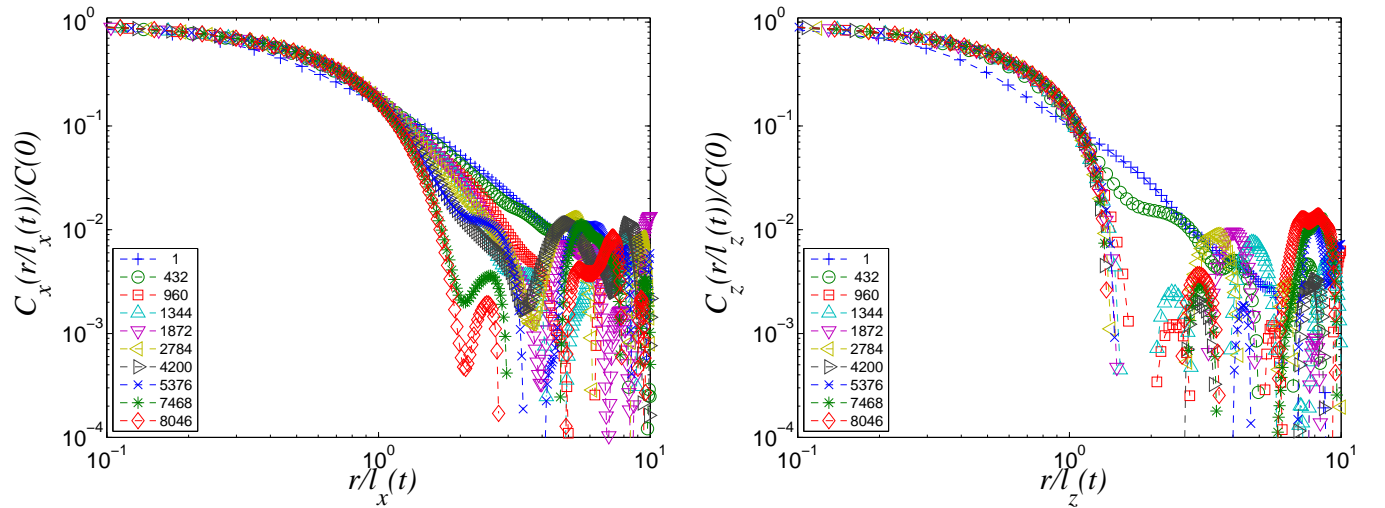


FIG. 5: (Colors online) Rescaled two-point correlation functions for $T = -3^\circ\text{C}$. Left: horizontal direction C_x Right: vertical direction C_z . The behavior at $T = -9^\circ\text{C}$ is similar.

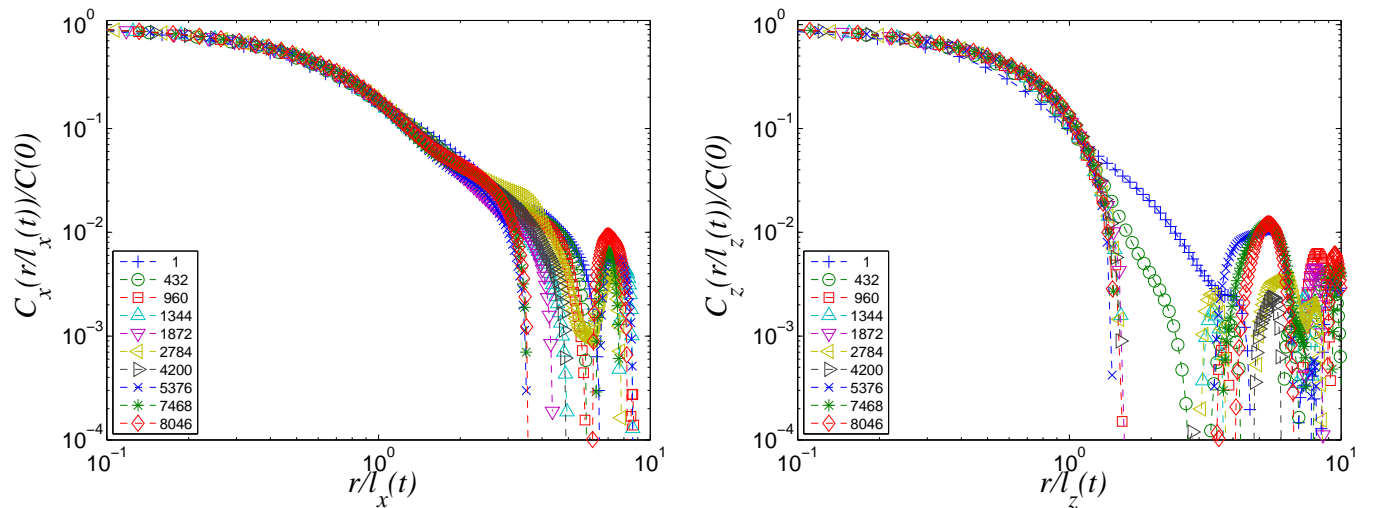


FIG. 6: (Colors online) Rescaled two-point correlation functions for $T = -19^\circ\text{C}$. Left: horizontal direction C_x Right: vertical direction C_z .

low temperature $T = -19^\circ\text{C}$ in Fig. 6. All plots are shown on a double logarithmic scale since the quality of the data collapse on larger scales remains usually unrevealed on a linear scale. For both temperatures a reasonable data collapse in z direction is already established after a short time and extends beyond the first zero crossing which is above $r/l_\alpha(t) \approx 1$. In contrast in x direction the scaling is poor and extends hardly beyond $r/l_\alpha(t) \approx 1$. Only at the very late stage after almost one year the quality of the scaling is comparable to that in z direction. In any case, the rescaling behavior of C is poor, indicating the absence of dynamic scaling and the existence of different relevant length scales.

2. Initial condition and final state

To shed additional light on the initial condition and the final states obtained after the entire year of coarsening the correlation functions for both states are compared for all temperatures in Fig. 7. Initially, correlations clearly exist beyond $r/l_\alpha(t) \approx 1$ in all three coordinate directions. The decay can approximately be described by a power-law with an exponent $C(r/l_\alpha(t)) \sim (r/l_\alpha(t))^{-\beta}$ with $\beta = 1.8$. This behavior is not very striking and extends only over a range of

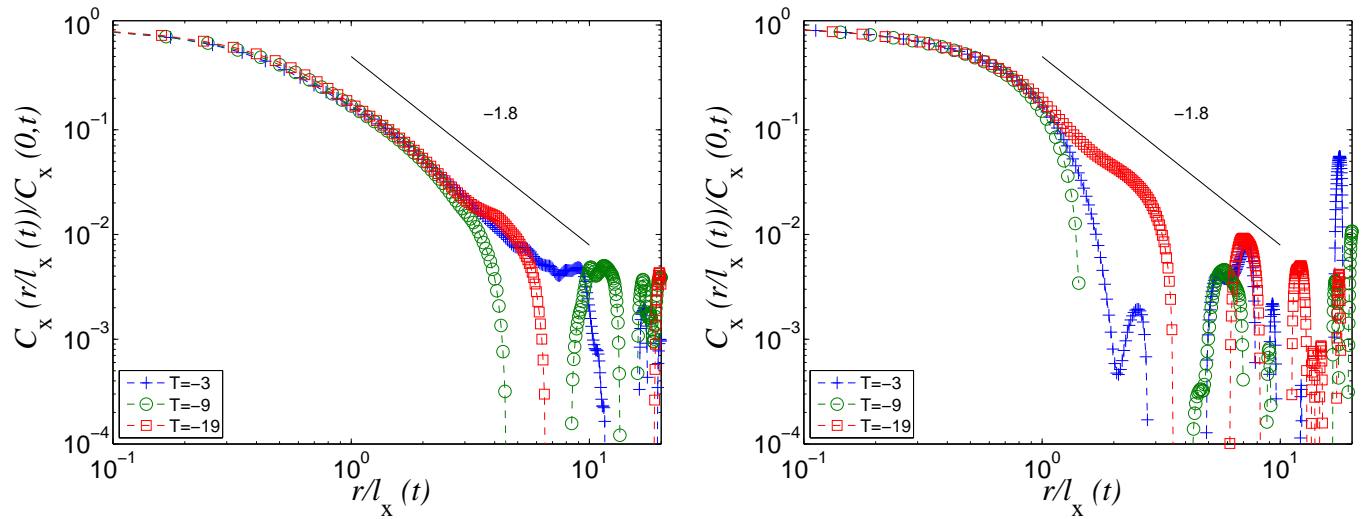


FIG. 7: (Colors online) Rescaled correlation functions of the initial (left) and the final state (right) for all temperatures.

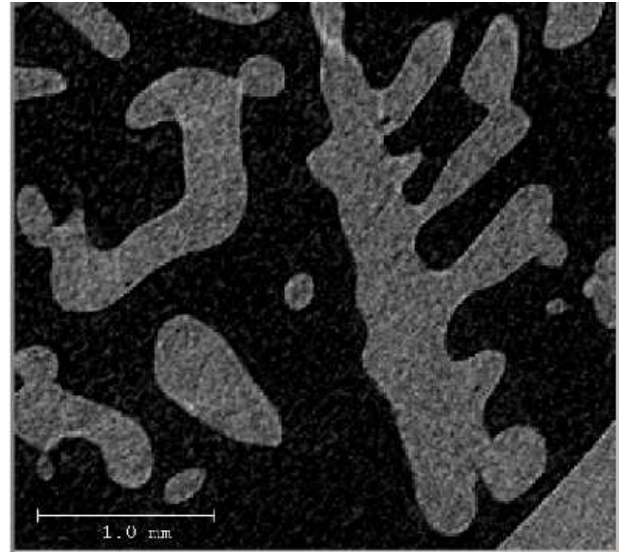
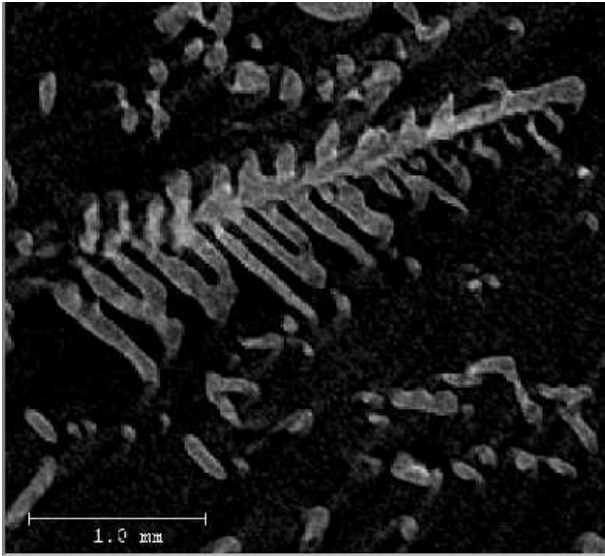


FIG. 8: Dendritic structures in snow at $T = -19^\circ\text{C}$ in the initial condition (left) and after one year (right) found in the $x - y$ plane. Note that the structures are not identical.

one magnitude. However, it clearly indicates the presence of correlations on scales large compared to $l_\alpha(t)$. The origin of this order is revealed by a closer, visual inspection of the sample, which reveals the presence of dendritic structures, cf. Fig. 8. For the lowest temperature the structures persist throughout the entire year. Again by (subjective) visual inspection we confirm that after one year at $T = -19^\circ\text{C}$ dendrites can only be found in the $x - y$ plane, cf. Fig. 8. whereas we could not find dendritic structures from views in the $x - z$ or $y - z$ plane. This is in agreement with the behavior found for the correlation function in Fig. 6: in x direction (also in y direction, not shown) at $T = -19^\circ\text{C}$ the initial power-law is still visible in form of a knee-like feature prior to the first zero crossing of the correlation function. In contrast in z direction any signature of the initial power-law correlations immediately disappears.

Before investigating the time evolution of the correlation lengths in detail we shall consider the distribution of ice thicknesses.

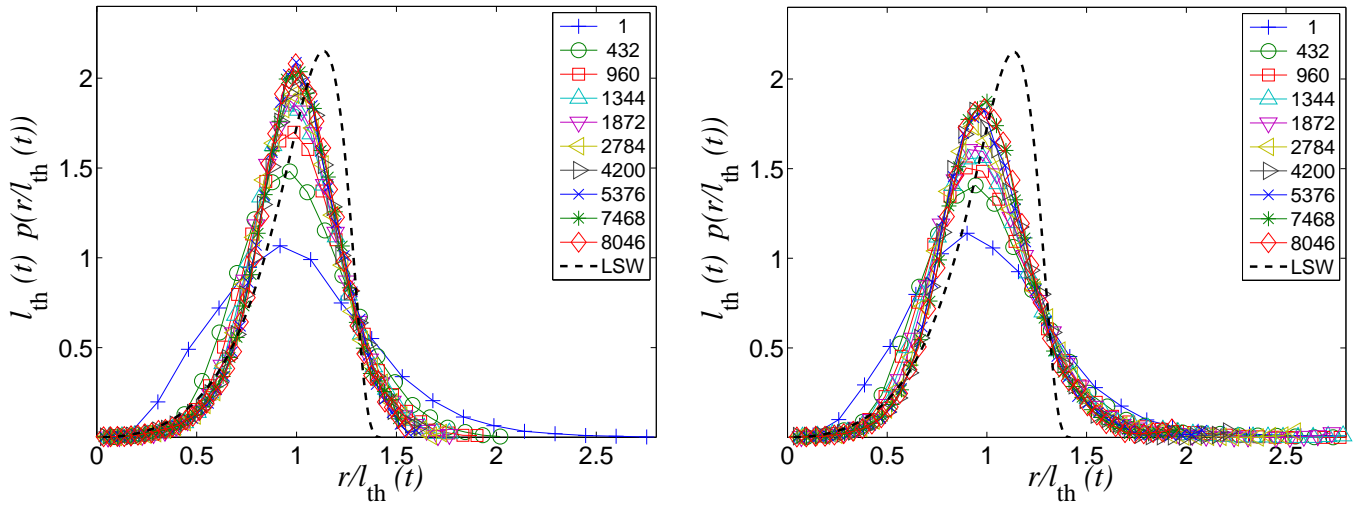


FIG. 9: (Colors online) Rescaled ice thickness distribution functions for $T = -3^\circ\text{C}$ (left), and $T = -19^\circ\text{C}$ (right).

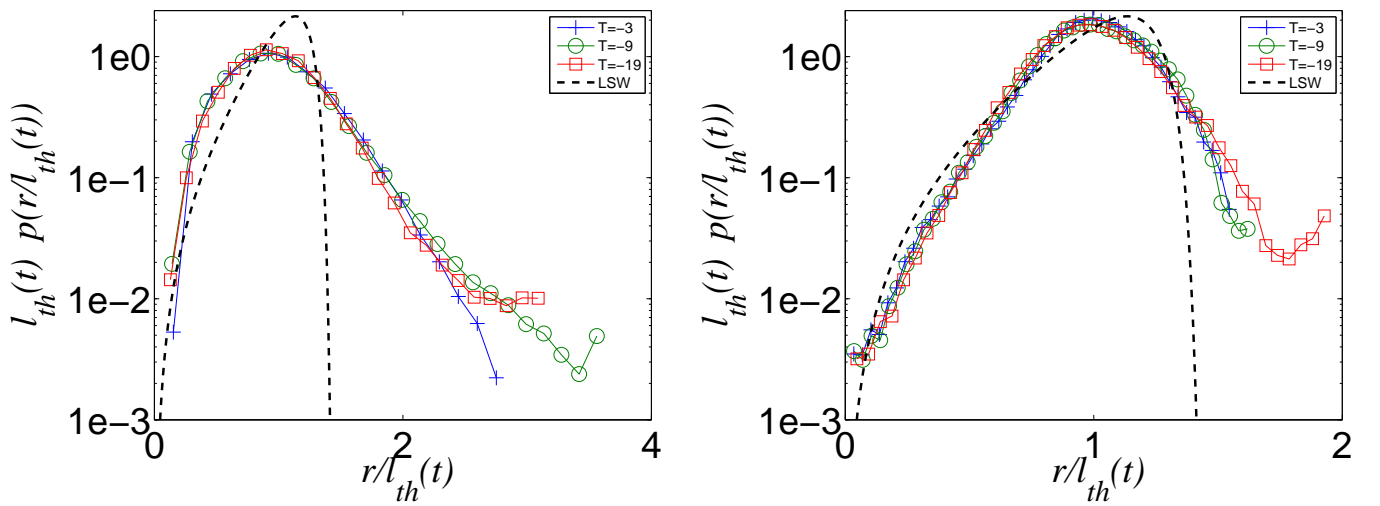


FIG. 10: (Colors online) Rescaled ice thickness distribution of the initial (left) and the final state (right).

D. Ice thickness distribution

1. Scaling

The ice-thickness distribution (7) is computed from the vendor software of the CT device by a distance transform of the ice phase [26]. The evolution of the rescaled (by the mean l_{th}) thickness distributions is given in Fig. 9. Since the thickness is a measure for an approximation of the structure by spheres, we also compare the thickness distribution to the classical radius distribution from Lifshitz and Slyozov [11] which is additionally plotted in Fig. 9. Again we concentrate on the comparison between $T = -3, -19^\circ\text{C}$.

2. Initial and final state

The ice-thickness distribution of the initial and final states are shown in Fig. 6 on a double logarithmic scale. It is difficult to reveal the existing correlations beyond $r/l_{\alpha}(t) \approx 1$ from the dendrites in the thickness distribution. This

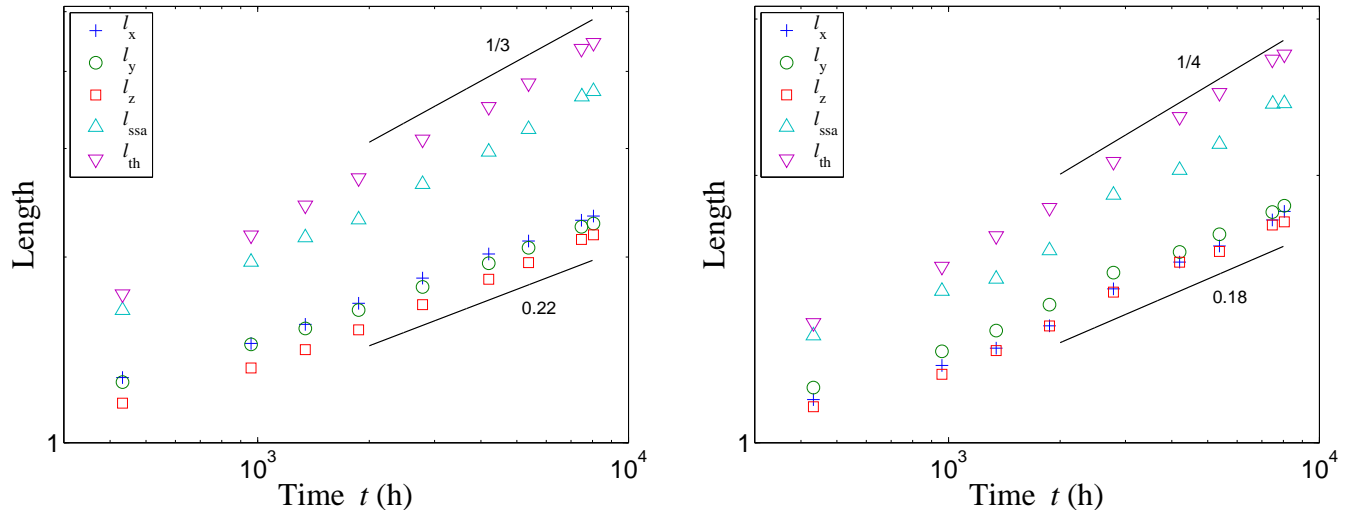


FIG. 11: (Colors online) Time evolution of the interfacial correlation lengths l_{th} , the ice thickness l_{ssa} , and the (inverse) specific surface area l_{ssa} at $T = -3^\circ C$ (left) and $T = -19^\circ C$ (right).

is due to its incapability of detecting the largest axis of anisotropic filaments. Therefore the interpretation of the tails of the distribution is somewhat subtle. Since $p_{th}(r, t)$ is an isotropic measure, the emerging anisotropy detected by the correlation function in different coordinate directions also remains unrevealed.

E. Length scales

Finally we compare the time evolution of all length scales defined in Sec. III which are derived from $C(r, t)$ and $p_{th}(r, t)$.

First we compare the interfacial correlation lengths l_α , the mean thickness l_{th} and the (inverse) specific surface area per ice volume l_{ssa} . For a better comparison we normalize all lengths by their initial values since absolute values of growth rates are not of interest in the present study. The various length scales are shown in Fig. 11. All of them show reasonable power law behavior with two different exponents which are given as straight black lines as a guide to the eye.

Finally, we evaluate the first zeros $l_{0,\alpha}$ of the correlation function in x and z direction in Fig. 12, again normalized by their initial values. Interestingly, a completely different, non-monotonic behavior is observed: The first zero of the $C_z(r, t)/C_z(0, t)$ always decreases in the beginning reaches a minimum after two time steps and increases subsequently. The time at minimum coincides with the beginning of the onset of data collapse of the z -correlation function $C_z(r, t)/C_z(0, t)$ observed in Fig. 5,6. In contrast, the first zeros of $C_x(r, t)/C_x(0, t)$ always display transient behavior in the beginning which is difficult to characterize. After attaining a maximum at intermediate times all scales seem to follow the slow growth of the z scales at the very late stage where all zeros grow in unison.

V. DISCUSSION

Our starting point of the discussion is the usual assumption of dynamic scaling during isotropic coarsening [19] which manifests itself in a scaling form

$$C_\alpha(r, t) = f(r/l(t)) \quad (9)$$

for the correlation function at long times independent of the direction α . Our measured correlation functions clearly reveals the breakdown of dynamic scaling during isothermal metamorphism of snow. This indicates a coupling between several length scales which has to be elucidated.

Our first result is the existence of different classes of length scales which can all be described by a power law, however with different exponents, cf. Fig. 11. This is precisely the behavior reported in [25] for the coarsening of fractal clusters as exemplified by the late stage dynamics of the Cahn-Hilliard equation. The key ingredient is the

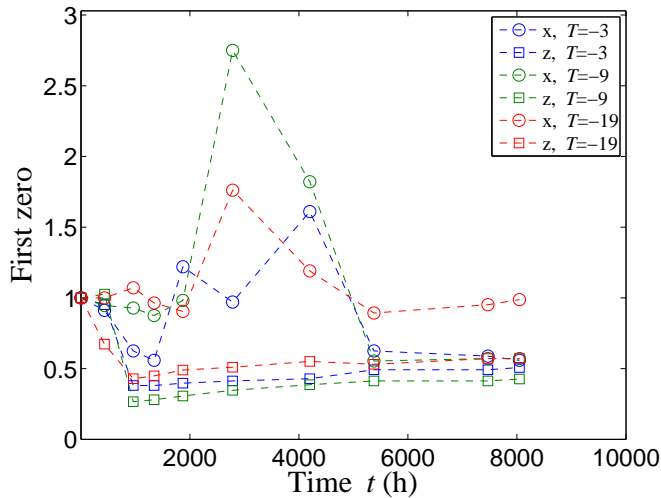


FIG. 12: (Colors online) Time evolution of the structural correlation lengths $l_{0,\alpha}$ for $\alpha = x$ (circles) and $\alpha = z$ (squares) at all temperatures.

presence of power law correlations in the initial conditions which gives rise to an additional relevant length scale during coarsening. In our case the initial conditions contain dendritic structures which survive the mechanical fragmentation process (sieving) during sample preparation. These structures are revealed by signatures of a power law tail in the correlation function well above the interfacial correlation length which is set by $r/l_\alpha(t) \approx 1$, cf. Fig. 5. The decay can roughly be described by $C(r, 0) \sim r^{-1.8}$, cf. Fig. 7. These correlations survive in form of the knee-like feature in the correlation function (cf. Fig. 5,6) over a large extent of time, as predicted in [25]. Visually the small scale dynamic in Fig. 5 is pinned at the initially immobile large-scale features (arms of the dendrites) which slows down the growth of small scales. Only in z direction the knee-like feature disappears almost immediately after two time steps and the correlation function exhibits reasonable data collapse up to its second zero crossing.

At high temperatures ($T = -3^\circ\text{C}$) the observed exponent values in Fig. 11 are close to $1/z = 0.33$, $1/z = 0.22$. The smaller value for $l_\alpha(t)$ is in agreement with that obtained in [25]. We note, that our definition of $l_\alpha(t)$ coincides with that given in their work, though our definition of the correlation function differs. The authors in [25] consider the two-point correlation function of a single, fractal cluster with respect to the origin which decays to zero for large distances. However, we are dealing with a collection of those clusters and a system which is homogeneous on large scales. Accordingly the two-point correlation function exhibits a non-zero value at large arguments, and therefore we have defined $C(r)$ to be the *covariance* of the random microstructure which tends to zero for large arguments. The larger of our power-law exponents is close to the LS value $z = 3$. We follow [25] and attribute this behavior to the signatures of locally conserved order parameter dynamics which is apparently detectable only in some length scales.

At low temperatures, cf. Fig. 11, the scenario is qualitatively identical to the high temperature case, only the values of the exponents have changed indicating a different underlying dynamics. Here, l_{th} and l_{ssa} follow an evolution which is close to $z = 1/4$ whereas the exponent for the interfacial correlation lengths l_α are again well below this value. A dynamic exponent $z = 1/4$ is characteristic for surface diffusion [28]. This is consistent with the observations in [2] where surface diffusion on ice is effectively damped above $T = -15^\circ\text{C}$. On general grounds one may expect however, that surface diffusion is only an intermediate dynamical regime since the $l \sim t^{1/3}$ scaling of evaporation-condensation will eventually always dominate the $l \sim t^{1/4}$ of surface diffusion. Thus it is likely that even at low temperatures a terminal LS value of $z = 3$ is attained at even later times. These time scales are however difficult to achieve experimentally. In addition, it is reasonable to expect that the crossover time scale where initial conditions of the surface correlation length have died out and the intermediate surface diffusion or the terminal evaporation-condensation dynamics is attained will itself increase with decreasing temperature. Thus, effective (time dependent) dynamic exponents $z(t) := d \ln(l)/d \ln(t)$ are measured, cf. [29] and an apparently continuous increase of the measured exponents with decreasing temperature is likely to occur. In analogy, to the high temperature case we attribute the exponent z which is obtained from l_{th} and l_{ssa} to the true dynamic behavior whereas $l_\alpha(t)$ is attributed to an anomalous behavior with a larger z .

If for the high temperature case the observed exponent $z = 3$ is regarded as the true dynamic behavior it is interesting to discuss how such a value characteristic for a locally conserved order parameter can be physically realized in our system. A suitable order parameter for the solidification phase field would be the density difference between ice and

vapor. Nominating evaporation-condensation as the dominant mechanism of mass transport does immediately imply a locally conserved dynamics for the order parameter. It is rather the fact that the evaporation-condensation dynamics is limited by the intermediate diffusion which ultimately fixes $z = 3$ [11]. If instead the evaporation-condensation dynamics were limited by the interface reaction one would end up with $z = 2$ [11, 12]. In the reaction limited regime diffusion can be regarded as infinitely fast, hence evaporated mass is immediately available for condensation at *remote* parts of the structure only subject to a global mass conservation. This effectively translates into an order parameter, which is only globally conserved which still leads to $z = 2$ [11], similar to the dynamics in the absence of any conservation law. The reaction limited case requires a small condensation coefficient [3], [8] on the interface and thus our result $z = 3$ is consistent with diffusion-limited evaporation-condensation.

Despite the absence of dynamic scaling, all length scales discussed so far still display a monotonic increase and can be reasonably well described by a power law which is the same for all coordinate directions. A completely different behavior is observed for the structural correlation lengths $l_{0,\alpha}$, which is non-monotonic and anisotropic. Remarkably, the observed anisotropy between the rescaling properties of $C(r, t)$ in z and x direction (Fig. 5,6) has no influence on the evolution of the interfacial correlation lengths l_α in the respective directions, cf. Fig. 11. This implies that the dynamics on the smallest scales remains isotropic if prefactors are neglected. This holds true at all temperatures and suggests that the anisotropy emerges from larger scales. This is confirmed by the evolution of the first zero crossing $l_{0,\alpha}$ of $C_\alpha(r, t)/C(0, t)$ which displays a complicated, anisotropic behavior. Usually, the zero crossing is interpreted as a typical domain size. Hence the vector $\Omega(t) \sim (l_{0,x}, l_{0,y}, l_{0,z})$ can be interpreted as an oriented structural unit of the ice network on scales larger than the previously discussed interfacial scale l_α . The dynamics of $\Omega(t)$ characterizes the evolution of some orientational order which does not show any qualitative differences between different temperatures, cf. Fig. 12: The z component of $\Omega(t)$ always decreases rapidly followed by a slow monotonic increase. The rapid decrease might be caused by some rotational motion under gravity. This might be corroborated by the fact that after one year the long arm of the dendrite is predominantly found in the $x - y$ plane. In contrast the x, y components of Ω show initially some transient behavior which is followed by a maximum where correlations roughly double when compared to the initial value. The temporal resolution is too coarse to investigate this phenomenon in quantitative detail but the qualitative features of the evolution are present at all temperatures. A quantitative investigation of these structural rearrangements, their possible *impact* on modulations of the bulk densification rate and their possible *initiation* by interfacial scale coarsening is left for future work.

Finally, we comment on the connection between the observed properties of the correlation function and interfacial curvature distributions which are often used to characterize the evolution of snow [8, 15]. The small scale expansion of the correlation function $C(r)$ for smooth but otherwise arbitrary microstructures can be written as $C(r) = (\phi - \phi^2) - (s/4)r - F[H, K]r^3 + \dots$ in terms of the volume fraction ϕ , specific surface area s and the mean and Gaussian curvature fields $H(x)$ and $K(x)$, respectively (see e.g. [22, Ch. 2]). Details which are irrelevant for the present argument are subsumed in the functional F . The expansion implies that the observed breakdown of dynamic scaling beyond the interface scale $r = 1/s$ is equivalent to the fact that the typical curvatures H, K have a different dynamic evolution as the specific surface area s and are more likely influenced by larger scale structural re-arrangements. Hence, the absence of scaling for the curvature distributions observed in [8] is in agreement with the absence of scaling in the correlation function at larger scales. Our analysis above suggests that this is an implication of the structural reorganization at larger scales and thus cannot be predicted by coarsening mechanisms alone. Previous work on isothermal metamorphism has usually focused on a single length scale $1/s$ and its interpretation in terms of modified LSW approaches. This is equivalent to neglect correlations of the density beyond the smallest interfacial scales. This appears to be insufficient due to the existence of different relevant length scales which are influenced by memory effects of initial conditions or gravity. A first attempt to include gravity in isothermal metamorphism has been done in Monte-Carlo simulations [17]. Future effort in this direction is highly desirable.

VI. CONCLUSIONS

We have investigated isothermal metamorphism of snow as an example of a material undergoing interfacial relaxations on the smallest scales with concurrent structural relaxations on larger scales. If the initial conditions contain density correlations on length scales which are large compared to the interfacial correlation length strong memory effects of the initial state can be expected. This appears to be one of the reasons for the breakdown of dynamic scaling for coarsening of snow.

The overall behavior of the interfacial relaxation is consistent with coarsening of fractal clusters. The underlying dynamics is governed by diffusion-limited evaporation-condensation with $z = 3$ at high temperatures and surface diffusion with $z = 4$ at low temperatures. In addition the dynamics at the scale of a typical, structural domain size displays a rather complex, non-monotonic behavior. The latter is attributed to structural relaxations of the ice network under the influence of gravity. Apparently, the strong variations of the dynamics on larger scales leave the

interfacial phase ordering nearly unaffected. Vice versa it poses the interesting question how large scale, structural mobility of the system can effectively be induced by interfacial coarsening.

Acknowledgments

We gratefully acknowledge the valuable support of Matthias Jaggi and Stephen Steiner during the experiments in the cold lab.

-
- [1] Y. Saito, *Statistical physics of crystal growth* (World Scientific (Singapore, London), 1996).
 - [2] K. Libbrecht, *J. Cryst. Growth* **247**, 530 (2003).
 - [3] K. Libbrecht, *Rep. Prog. Phys.* **68**, 855 (2005).
 - [4] C. Westbrook, R. Ball, P. Field, and A. Heymsfield, *Phys. Rev. E* **70** (2004).
 - [5] H. Löwe, L. Egli, S. Bartlett, M. Guala, and C. Manes, *Geophys. Res. Lett.* **34** (2007).
 - [6] L. Arnaud, M. Gay, J.-M. Barnola, and D. P., in *Physics of Ice Core Records*, edited by T. Hondoh (Hokkaido University Press, Hokkaido, Japan, 2000), pp. 263–268.
 - [7] F. Domine, T. Lauzier, A. Cabanes, L. Legagneux, W. Kuhs, K. Techmer, and T. Heinrichs, *Microsc. Res. Techniq* **62**, 33 (2003).
 - [8] L. Legagneux, A. Taillandier, and F. Domine, *J. Appl. Phys.* **95**, 6175 (2004).
 - [9] L. Legagneux and F. Domine, *J. Geophys. Res. Earth* **110** (2005).
 - [10] T. U. Kaempfer and M. Schneebeli, *J. Geophys. Res. Atmos.* **112** (2007).
 - [11] I. Lifshitz and V. Slyozov, *J. Phys. Chem. Solids* **19**, 35 (1961).
 - [12] C. Wagner, *Z. Elektrochem.* **65**, 581 (1961).
 - [13] J. Yao, K. Elder, H. Guo, and M. Grant, *Phys. Rev. B* **47**, 14110 (1993).
 - [14] J. R. Blackford, *J. Phys. D Appl. Phys.* **40**, R355 (2007).
 - [15] F. Flin, J. Brzoska, B. Lesaffre, C. Cileou, and R. Pieritz, *J. Phys. D Appl. Phys.* **36**, A49 (2003).
 - [16] F. Flin, J. Brzoska, B. Lesaffre, C. Coleou, and R. Pieritz, in *Ann. Glaciol.*, edited by P. Fohn (2004), vol. 38 of *Ann. Glaciol.*, pp. 39–44.
 - [17] R. Vetter, S. Sigg, H. M. Singer, D. Kadau, H. J. Herrmann, and M. Schneebeli, *Europhys. Lett.* **89**, 26001 (2009).
 - [18] L. Ratke and P. Voorhees, *Growth and coarsening* (Springer, New York, 2002).
 - [19] A. Bray, *Adv. Phys.* **43**, 357 (1994).
 - [20] Y. Kwon, K. Thornton, and P. W. Voorhees, *Phys. Rev. E* **75** (2007).
 - [21] P. Debye and A. Bueche, *J. Appl. Phys.* **20**, 518 (1949).
 - [22] S. Torquato, *Random heterogeneous materials* (Springer, New York, 2002).
 - [23] H. Nakamura, *Tech. Rep.*, Bosai Kagaku Gijutsu Kenkyujo Kenkyu Hokoku (Report of the National Research Institute for Earth Science and Disaster Prevention) (1978).
 - [24] T. Kaempfer, M. Schneebeli, and S. Sokratov, *Geophys. Res. Lett.* **32** (2005).
 - [25] A. Lipshtat, B. Meerson, and P. Sasorov, *Phys. Rev. E* **65** (2002).
 - [26] T. Hildebrand and P. Ruesegger, *J. Microscopy* **185**, 67 (1997).
 - [27] M. Kerbrat, B. Pinzer, T. Huthwelker, H. W. Gaeggeler, M. Ammann, and M. Schneebeli, *Atmos. Chem. Phys.* **8**, 1261 (2008).
 - [28] R. Balluffi, S. Allen, and W. Carter, *Kinetics of materials* (Wiley-Interscience (Hoboken, N.J), 2005).
 - [29] D. Huse, *Phys. Rev. B* **34**, 7845 (1986).